February 2006

Raghavan, V., Pope, D.N., Howard, D. and Gogos, G. "Surface Tension Effects during Low Reynolds Number Methanol Droplet Combustion," Combustion and Flame, accepted (2006)

Surface Tension Effects during Low Reynolds Number Methanol Droplet Combustion

a full-length article by

Raghavan Vasudevan[‡], Daniel N. Pope[†], Damon Howard[⌂] and George Gogos[*]

Accepted for publication in
Combustion and Flame

[*]Corresponding author: George Gogos
University of Nebraska-Lincoln
Department of Mechanical Engineering
N104 Walter Scott Engineering Center
Lincoln, NE. 68588-0656
Tel: 402-472-3006 Fax: 402-472-1465
E-mail: ggogos@unl.edu

[†] Assistant Professor
University of Minnesota Duluth
Department of Mechanical and Industrial Engineering
105 VKH, 1305 Ordean Court
Duluth, MN. 55812-3042

[‡] Post Doctoral Research Associate
Department of Mechanical Engineering
University of Nebraska-Lincoln

[⌂] Currently working with
Bettis Atomic Laboratories,
Pittsburgh, Pennsylvania

Abstract

A numerical investigation of methanol droplet combustion in a zero-gravity, low-pressure and low-temperature environment is presented. Simulations have been carried out using a predictive, transient and axisymmetric model, which includes droplet heating, liquid-phase circulation and water absorption. A low initial Reynolds number (Re_0=0.01) is used to impose a weak gas-phase convective flow, introducing a deviation from spherical symmetry. The resulting weak liquid-phase circulation is greatly enhanced due to surface tension effects, which create a complex, time-varying, multi-cellular flow pattern within the liquid droplet. The complex flow pattern, which results in nearly perfect mixing, causes increased water absorption within the droplet, leading to larger extinction diameters. It is shown that, for combustion of a 0.43 *mm* droplet in a nearly quiescent environment (Re_0=0.01) composed of dry air, the extinction diameter is 0.11 *mm* when surface tension effects are included, and 0.054 *mm* when surface tension effects are neglected. Experimental work available in the literature for a 0.43 *mm* droplet reported extinction diameters in the range of 0.16 to 0.19 *mm*. Results for combustion in a nearly quiescent environment (Re_0=0.01) with varying initial droplet diameters, (0.16 to 1.72 *mm*), show that including the effect of surface tension results in an approximately linear variation of the extinction diameter with the initial droplet diameter, which is in agreement with theoretical predictions and experimental measurements. In addition, surface tension effects are shown to be important even at initial Reynolds numbers as high as 5.

Keywords: surface tension, extinction, water absorption, methanol, droplet combustion

1 Introduction

To better understand the fundamental characteristics of isolated droplet burning, several investigators have studied droplet combustion by employing methanol as the fuel. Methanol offers several advantages, such as a simple chemical composition, non-sooting behavior and a well understood oxidation mechanism. However, the complication in using methanol droplets is the absorption of water into the droplet due to the high polarity of both water and methanol molecules, which causes them to readily mix. Water initially present in the ambient and/or produced through combustion, condenses onto the droplet surface. The water at the droplet surface may either vaporize or be transported to the droplet interior, via mass diffusion, which may be enhanced by liquid-phase circulation. The condensation and transport of water results in a continuous increase in the water content on the droplet surface and within the droplet interior. At a particular point in time, the water content increases to a level where the vaporizing methanol cannot sustain the combustion reaction, leading to flame extinction. Thus, water absorption grossly affects the burning characteristics of methanol droplets.

Experimental investigations of methanol droplet combustion have employed either unsupported droplets [1-5] or droplets suspended from thin fibers [6, 7]. Both suspended and unsupported droplet experiments are often conducted in a quiescent, microgravity environment [1, 2 and 4-7] in order to approach spherically symmetric conditions and better understand the fundamental phenomena associated with isolated droplet burning. However, there are many difficulties in attaining spherically symmetric conditions. Disturbances from various sources such as droplet drift velocity (of the order of 1 ~ 4 mm/s), deployment of the droplet, effect of the fiber used to suspend the droplet and ignition of the droplet are present. These disturbances

cause a non-uniform distribution of chemical species and temperature along the droplet surface resulting in a deviation from spherically symmetric conditions.

Among the main objectives of the above experimental studies [1-7] were the characterization of the extinction diameter, evaporation constant, and lifetime of methanol droplets. Many of these experiments were carried out in drop towers [1, 2, 4, 5 and 7] to generate microgravity conditions. The use of drop towers restricts the total available combustion time. The limited combustion time is often insufficient to observe extinction when the ambient is composed of air [2, 4]. To overcome this difficulty, oxygen mixed with inert gases other than nitrogen have been used in some drop-tower experiments [2, 5] to shorten the combustion time and allow for the observation of droplet extinction. Experimental studies that varied the initial water content in the ambient environment [3] and in the liquid droplet [4, 6] have addressed the influence of these factors on the absorption of water by methanol droplets. It has been shown experimentally that the absorption of water causes a methanol droplet to extinguish at a larger diameter than a hydrocarbon droplet of the same initial diameter [1, 6 and 8], and that, for methanol droplets, the extinction diameter varies approximately linearly with the initial droplet diameter [6].

Several investigators, such as Marchese et al. [4], Shaw [9], Zhang et al. [10], and Marchese and Dryer [11], have conducted analytical and numerical studies of spherically symmetric methanol droplet combustion. The asymptotic analysis of Zhang et al. [10] and the numerical results of Marchese and Dryer [11] both show that considering only diffusion transport within the methanol droplet leads to the under-prediction of extinction diameter when compared to experimental results. Investigators have concluded that internal mixing is responsible for additional water within the droplets, which leads to much larger extinction

diameters than those predicted through one-dimensional models. The sources of internal mixing are likely multifold, but are not due to relative gas/liquid convection effects at the interface [4]. A small relative velocity between the droplet and surrounding gas-phase, however, could be one of the disturbances that could trigger surface tension effects, which can lead to intense internal mixing, as will be discussed below. The asymptotic analysis of Shaw [9] indicates that water transport influences conditions in and near the flame and the burning rates of initially-pure methanol droplets. The mass fraction of water in the droplet is about 40% to 80% at extinction [10] and water transport due to diffusion alone cannot account for the large quantities of water absorbed. Marchese and Dryer [11] used detailed chemical kinetics in their numerical model to predict extinction of bicomponent droplets of methanol and water. However, the extinction diameters have been under-predicted and a particular parameter (liquid phase Peclet number) was adjusted in order to get reasonable extinction diameters. Marchese and Dryer [11] reported that the unadjusted value for the liquid phase Peclet number (defined as the ratio of the droplet surface regression velocity to the effective diffusion velocity within the liquid droplet) is typically greater than 20 for methanol burning in air. Their numerical results were in agreement with the experiments when it was speculated that sufficient internal liquid phase motion was present to reduce the effective liquid mass Peclet number to the order of one. It has been suggested in the literature that surface tension gradients could be responsible for "perfect mixing" [10 and 11], which can account for the amount of water measured in the experiments.

Axisymmetric numerical models have also been developed and reported in the literature. Aharon and Shaw [12], in their numerical investigation of bi-component droplet using an axisymmetric droplet evaporation model, have concluded that the thermal Marangoni effect (surface tension gradient due to temperature gradient) has a stabilizing effect and the solutal

Marangoni effect (surface tension gradient due to composition gradient) has a destabilizing effect. Recently, Dwyer et al. [13-15] numerically investigated surface tension effects for both vaporizing and combusting methanol droplets with their axisymmetric model. Their results show that variations in surface tension due to composition and temperature can have a strong effect on the flow patterns in the liquid droplet. Shih and Megaridis [16] considered the thermal Marangoni effects on droplet evaporation in a convective environment. They have concluded that surface tension gradients due to spatial variations of temperature along the interface have a profound impact on droplet dynamic behavior. Gogos and coworkers [17-20] and Raghavan et al. [21] developed axisymmetric droplet combustion models and predicted quantities like mass burning rates, flame shapes, extinction velocities and extinction diameters. Axisymmetric configurations have also been studied experimentally by Sami and Ogasawara [22] using the porous sphere technique to simulate quasi-steady methanol droplet burning within a convective environment. Flame shapes, mass burning rates and extinction velocities have been measured.

The literature strongly suggests that during microgravity droplet combustion experiments, sources of disturbances like droplet drift velocity, droplet deployment, droplet support fibers and droplet ignition cause deviation from intended spherical symmetry. As a result, concentration and temperature gradients along the droplet surface have been present in the microgravity experiments. These gradients enable surface tension forces to come into play. The surface tension causes rapid and complex circulatory flow patterns within the liquid phase, which enhance the amount of water absorbed by the droplet. The present study is aimed at reporting the effect of surface tension on the absorption of water in the liquid-phase during the combustion of an isolated methanol droplet in air. The predictive, transient, two-phase, axisymmetric model used in the present study includes surface tension effects, so as to accurately model the thorough

mixing and water absorption taking place in the liquid-phase. The present numerical investigation clearly shows how surface tension effects influence the liquid phase mixing, the extinction diameter, the liquid-phase flow patterns and the amount of water absorbed. Surface tension effects are shown to dominate free stream convection, even at initial Reynolds numbers as high as 5. The variation of extinction diameter with the initial droplet diameter has been presented for both the cases that include and exclude surface tension effects, to clearly show that the model with surface tension effects predicts much larger extinction diameters, in closer agreement with experimental results. The description of the numerical model and its validation along with detailed discussions of results for low initial Reynolds numbers are presented in the subsequent sections.

2 Numerical Model

The numerical model used in this work is an axisymmetric, transient model which solves for both liquid- as well as gas-phase mass, momentum, species and energy conservation equations. The main features of this model are the inclusion of multi-component diffusion in both the phases, a comprehensive method to deal with the interface (including surface tension effects), and variation of thermo-physical properties as a function of temperature and species concentration in both the phases. A detailed description of the model and its validation for n-heptane droplet combustion is given in Pope et al. [19]. The model has been modified for the present study to include methanol as the fuel, surface tension effects, and the liquid-phase conservation of species equation. A brief description of the model and the assumptions employed are given below.

The model simulates the combustion of a liquid methanol droplet undergoing evaporation and combustion in a low pressure, zero-gravity, convective environment of infinite expanse (Fig. 1). The free stream pressure (p_∞) and the free stream temperature (T_∞) are held constant. The effect of the suspension fiber used to suspend the droplet as in an experiment, is neglected. Other assumptions include: (1) axisymmetric, laminar flow, (2) spherical droplet shape, (3) zero coefficient of bulk viscosity and (4) thermal radiation, pressure diffusion, Dufour effect, Soret in the liquid-phase, viscous dissipation and pressure work are negligible.

The governing equations for the gas and liquid phases are the transient axisymmetric equations for continuity, conservation of species, conservation of energy and conservation of momentum, in $r-\theta$ spherical coordinates. A set of interfacial conservation equations couple the gas and the liquid phase. The details are given in [19]. The equation for continuity of shear

stress at the interface is of particular interest for this present study and is modified to include surface tension effects. It is given by,

$$\mu_{g,s}\left[\frac{\partial \mathrm{v}_\theta}{\partial r}+\frac{1}{r}\frac{\partial \mathrm{v}_r}{\partial \theta}-\frac{\mathrm{v}_\theta}{r}\right]_{g,s}+\frac{1}{r}\frac{\partial \sigma}{\partial \theta}\bigg|_s=\mu_{l,s}\left[\frac{\partial \mathrm{v}_\theta}{\partial r}+\frac{1}{r}\frac{\partial \mathrm{v}_r}{\partial \theta}-\frac{\mathrm{v}_\theta}{r}\right]_{l,s} \quad (1)$$

where the second term on the left-hand side is the surface tension gradient along the droplet surface. In the above equation subscripts *l* and *g* indicate the liquid phase and the gas phase, respectively, and the subscript *s* indicates the gas/liquid interface. In addition, in equation (1), v represents velocity, μ represents absolute viscosity and σ represents surface tension. The above equation together with the no-slip condition is used to obtain the tangential velocity at the droplet surface. The gas-phase diffusion velocities ($\mathbf{V}_i$), which depend upon concentration and temperature gradients for all *N* species, are solved according to the method presented by Pope and Gogos [17]. The liquid phase consists of a binary mixture of methanol and water, and the diffusion velocities are calculated using Fick's Law for ordinary diffusion alone. The binary diffusion coefficient is calculated as a function of mutual binary diffusion coefficients at very low concentrations, mole fractions of the species and a thermodynamic correction factor that depends upon composition and temperature for a binary mixture (Reid et al. [23]). The interface composition was determined using a low-pressure binary vapor-liquid equilibrium equation based upon the activity coefficients. The activity coefficients were calculated using the Wilson correlation [24]. Variable thermo-physical properties in the gas-phase were calculated using correlations from Reid et al. [23] and McBride et al. [25]. The liquid-phase properties were calculated using correlations from Reid et al. [23] as well as Teja [26] and Teja and Rice [27]. Surface tension for a pure component (methanol or water) is calculated from a temperature dependent curve-fit of experimental data [28]. A mixing rule based on composition [24] is used

to yield a temperature and composition dependent surface tension. Both the droplet surface composition and the droplet surface temperature play a role in determining surface tension. The method for calculating the surface tension has been validated against the work of Santos et al. [29]. Figure 2 shows the experimental results of Santos et al. [29] for water/methanol mixtures in thermodynamic equilibrium with air at 303.15 K along with results from the code used in this study. It is seen that agreement is good, especially in the region where the mole fraction of the fuel is above 0.6, which is the range for almost the entire droplet lifetime (see Results and Discussion Section).

A one-step overall reaction is used to model the combustion of methanol in air and is given below:

$$CH_3OH + 1.5\left(O_2 + 3.77N_2\right) \rightarrow CO_2 + 2H_2O + 1.5\left(3.77N_2\right) \qquad (2)$$

The resulting expression for the mass-based rate of production/destruction of species *i* per unit volume, given by, ω_i is written as:

$$\omega_i = W_i\left(\nu_i'' - \nu_i'\right)A\left(\frac{\rho Y_f}{W_f}\right)^a\left(\frac{\rho Y_o}{W_o}\right)^b \exp\left[\frac{-E_a}{R_u T}\right] \qquad (3)$$

In the above expression, W_i is the molecular weight of species *i*, and ν_i'' and ν_i' are the stoichiometric coefficients of species *i* as it appears as a product or reactant, respectively. The pre-exponential factor (A), activation energy (E_a) and the fuel and oxygen concentration exponents (*a* and *b*) used in the simulation have been taken from Westbrook and Dryer [30]. Quasi-steady simulations were performed to validate the global single step mechanism as discussed in the Validation Section.

The governing equations are discretized using the finite volume [31] and SIMPLEC [32] methods. Convection-diffusion is modeled using the power-law scheme [30]. A collocated grid is used with hyperbolic tangent stretching functions [33] used to cluster the grid points near the droplet surface in both the gas and the liquid phases. The discretized equations are solved using the Alternating Direction Implicit (ADI) with Tri-Diagonal Matrix Algorithm (TDMA). Iterations are performed within each time step until desired convergence is achieved. An adaptive time step has also been employed. Grid and domain independence studies have been carried out to ensure that the solution is independent of grid and domain. The lower and upper limits of time steps have been carefully sought so as to capture the physics during the entire evaporation and combustion processes in a computationally efficient manner.

The low ambient temperature results considered in the present work require a means of initiating ignition of the fuel vapor/air mixture that surrounds the droplet. Ignition is accomplished numerically by running the code for a few time steps so that, due to evaporation, a fuel vapor/air mixture builds up around the droplet. Energy is then added to an axisymmetric region upstream of the droplet via the source term in the conservation of energy equation. The addition of energy occurs over several time steps and is terminated when ignition takes place. A detailed discussion of the ignition process is given in the Droplet Ignition Transient Section. A similar procedure has been employed by Marchese and Dryer [11] for spherically symmetric droplet ignition.

3 Results and Discussion

The numerical model was used to investigate various cases of suspended (constant velocity) methanol droplet combustion at low Reynolds numbers, with and without surface tension effects. In order to neglect surface tension effects, the second term on the left-hand side of the interfacial continuity of shear stress equation has been dropped. Numerical results for initially pure methanol droplets at a uniform initial temperature (T_0) of 297 K undergoing combustion in a zero-gravity environment consisting of air with a freestream temperature (T_∞) and pressure (p_∞) of 300 K and 1 atm, respectively, are presented. The simulated droplet ignition transient is addressed followed by discussions of the model validation and the effects of varying initial Reynolds number (Re_0) and droplet initial diameter (d_0) on the numerical predictions.

3.1 Droplet Ignition Transient

Experimental results for droplet combustion are generally presented as a function of time after ignition. Thus, numerical simulations must either model the ignition process or assume a set of initial conditions that correspond to the already ignited state for the droplet. As previously stated, the current model simulates an external ignition source by first running the code for a few time steps so that, due to evaporation, a fuel/vapor air mixture builds up around the droplet, and then adding energy to a small axisymmetric region upstream of the droplet until ignition takes place.

The current work utilizes the experimental data obtained by Yang et al. [1] to validate the numerical model (discussed later). Yang et al. [1] presented data for methanol droplets with initial diameters ranging from 0.40 to 0.43 mm burning in quiescent air at room temperature and atmospheric pressure. Our numerical simulations are conducted with d_0 = 0.43 mm and the ambient and initial conditions previously noted. An initial Reynolds number of $Re_0 = d_0 U_\infty / \nu_\infty$ =

0.01, where U_∞ is the freestream velocity and ν_∞ is the kinematic viscosity evaluated at the freestream conditions, is selected to correspond to the nearly quiescent environment in the experimental work. The simulations for this case allowed the droplet to evaporate for approximately 1.5 ms before applying the external ignition source.

During the pure evaporation phase in dry air, the numerical results with and without surface tension are nearly identical. The only result that is noticeably affected when surface tension effects are included is the droplet circulation. At the start of the simulation, a weak clockwise circulation is induced in the droplet due to the slow convective flow surrounding the droplet. Figure 3 shows the dimensionless tangential velocity ($v_\theta^* = v_\theta/U_\infty$) and droplet surface temperature (T_s) distribution along the droplet surface at $t \approx 1.3$ ms after the start of the simulation. The weak clockwise circulation initially induced within the droplet remains throughout the evaporation phase when surface tension is neglected (dashed line, Fig. 3a). When surface tension effects are included, the weak clockwise circulation slows and eventually reverses direction as shown in Fig. 3a (solid line). The cause of this flow reversal is the variation of the surface tension at the droplet surface. The gradient of the surface tension along the droplet surface can be expressed in terms of the surface temperature and surface water mass fraction (Y_{ws}) gradients, as follows:

$$\frac{\partial \sigma}{\partial \theta} = \frac{\partial \sigma}{\partial T_s}\frac{\partial T_s}{\partial \theta} + \frac{\partial \sigma}{\partial Y_{ws}}\frac{\partial Y_{ws}}{\partial \theta} \qquad \textbf{(4)}$$

The first term in Eq. (4) represents the thermal Marangoni effect (which drives the liquid from hot to cold regions of the gas-liquid interface) and the second term represents the solutal Marangoni effect (which drives the liquid from low to high water mass fractions of the gas-liquid interface). Both cases shown in Figure 3 are for the initially pure evaporation phase in dry air.

Thus, the solutal Marangoni effect is absent. Evaporation of fuel at the droplet surface causes a reduction in the droplet surface temperature from its initial value of 297 K as shown in Fig. 3b. At this low Reynolds number (Re_0 = 0.01), T_s is approximately constant along the droplet surface and nearly identical for the two cases. However, even under weak convection, the upstream side of the droplet experiences enhanced cooling resulting in a temperature gradient of $\partial T_s/\partial\theta = O(10^{-4})$ K. This small temperature gradient causes a corresponding surface tension gradient that overcomes the very weak circulation generated when Re_0 = 0.01. The higher initial Reynolds number cases ($0.1 \leq Re_0 \leq 5$) discussed later, did not display this flow reversal during the evaporation phase. All of the combustion results in the present article are insensitive to modest variations in the initial pure evaporation period.

The external ignition source is added at 1.5 ms after the start of the simulation. Figure 4a shows a grayscale plot of the temperature distribution surrounding the droplet at t = 3 ms when surface tension is neglected. The axisymmetric region of energy addition is clearly visible. Figures 4b-d show the predicted variation of v_θ*, T_s and Y_{ws} along the droplet surface at t = 3 ms with and without surface tension effects. The high temperature region in the gas phase (Fig. 4a) causes heating of the front portion of the droplet (Fig. 4c) and water vapor produced in the gas phase condenses on the droplet surface (Fig. 4d). The ignition source also causes a drastic change in v_θ*. For the case neglecting surface tension, the maximum value of v_θ* increases from 0.015 (dashed line, Fig. 3a) during evaporation to approximately 5 (dashed line, Fig. 4b) shortly after the application of the ignition source. The reason for this large increase is the volumetric expansion that takes place near the front of the droplet which accelerates the clockwise circulation within the droplet (Fig. 4b). The effect of the external ignition source on v_θ* is even more pronounced when surface tension effects are included. The very weak counter-clockwise

flow with a minimum v_θ* of approximately -0.008 (solid line, Fig. 3a) that is present near the end of evaporation changes to a strong clockwise flow with a maximum v_θ* of over 400 (solid line, Fig. 4b) shortly after the application of the ignition source. This clockwise flow is partially caused by the volumetric expansion of gases noted earlier. However, Figure 4b shows that the strength of the flow is two orders of magnitude higher when surface tension effects are included. The sensitivity of σ with respect to T_s and Y_{ws} in equation (4) is such that the tangential velocity at the droplet surface is accelerated in the direction of decreasing T_s and increasing Y_{ws}. Figures 4c and 4d indicate that the distribution of T_s and Y_{ws} along the droplet surface should contribute to a clockwise and a counter-clockwise flow, respectively. Detailed numerical results around t = 3 ms indicate that the thermal Marangoni effect is approximately five times greater than the solutal Marangoni effect when the external ignition source is applied. The dominance of the thermal Marangoni effect during this period is caused by localized heating of the gas phase (Fig. 4a) which creates a large temperature gradient along the droplet surface (Fig. 4c). The solutal Marangoni effect depends on both the gradient of Y_{ws} and the sensitivity of σ with respect to Y_{ws}. Figure 2 indicates that σ is less sensitive to Y_{ws} when the water mass fraction is low. Since the application of the ignition source takes place over a relatively short time period, there is insufficient time for large quantities of water to condense on the droplet surface (Fig. 4d) and the resulting gradient of Y_{ws} is small. Thus, the magnitude of the solutal Marangoni effect is small relative to the thermal Marangoni effect during the period of energy addition.

The addition of energy is terminated when the maximum gas-phase temperature reaches 2000 K, at which point, combustion becomes self sustaining. As a result, energy addition is terminated at approximately t = 16.4 ms and t = 12.7 ms when surface tension effects are included and neglected, respectively. Figure 5a shows a grayscale plot of the temperature

distribution surrounding the droplet at t = 12.7 ms when surface tension is neglected. The flame is beginning to surround the droplet. Figures 5b-d show the predicted variation of v_θ*, T_s and Y_{ws} along the droplet surface when energy addition is terminated both with and without surface tension effects. A comparison of Figures 4c and 5c shows an increase in surface temperature due to droplet heating. Condensation of additional water vapor on the droplet surface and the increase in Y_{ws} is seen when comparing Figures 4d and 5d. The results that include surface tension effects are already showing signs of enhanced mixing. Figures 5c and 5d show that maximum values and gradients of T_s and Y_{ws} decrease when surface tension effects are included. This decrease is evident despite the fact that the results that include surface tension effects are at a slightly later time (t = 16.4 ms) than the results neglecting surface tension effects (t = 12.7 ms). The enhanced mixing caused by the strong clockwise circulation (solid line, Fig. 5b) communicates the higher values for T_s and Y_{ws} at the front of the droplet to the rear. The volumetric expansion of the gas phase along the trailing half of the droplet (Fig. 5a) causes a back pressure on the droplet. This backpressure is insufficient to overcome the strong clockwise circulation induced by the thermal Marangoni effect (solid line, Fig. 5b). However, the backpressure is sufficient to initiate a counter-clockwise flow in the trailing half of the droplet (in the vicinity of θ=120˚) when surface tension effects are neglected (dashed line, Fig. 5b). After the termination of energy addition, the flame continues to engulf the droplet, eventually forming an envelope flame.

An envelope flame is formed around the droplet at approximately t = 19.2 ms and t = 17.4 ms when surface tension effects are included and neglected, respectively. Figure 6a shows a grayscale plot of the temperature distribution surrounding the droplet at t = 17.4 ms when surface tension is neglected. The flame is closer to the droplet surface at the rear of the droplet

and has not approached spherical symmetry. During the formation of the envelope flame, the volumetric expansion of the gas phase near the rear of the droplet is violent enough to cause counter-clockwise circulation when surface tension effects are neglected (dashed line, Fig. 6b). When surface tension effects are included, this same volumetric expansion contributes to the formation of a small region of counter-clockwise circulation near the trailing edge of the droplet (solid line, Fig. 6b). The appearance of the envelope flame allows for heating of the entire droplet surface and creates a "source" of water vapor that surrounds the droplet. Therefore, the case that includes surface tension effects shows a decrease in the magnitude of the temperature difference along the droplet from approximately 12 K when energy addition terminates (solid line, Fig. 5c), to approximately 2 K when an envelope flame is formed (solid line, Fig. 6c). The resulting decrease in the gradient of T_s lessens the thermal Marangoni effect. Detailed analysis of the numerical results indicates that when the envelope flame forms, the solutal and thermal Marangoni effects are of the same order. The closeness of the flame to the rear of the droplet causes an increased rate of water condensation along the trailing edge. When surface tension effects are included, the result is a higher Y_{ws} along the trailing edge of the droplet (solid line, Fig. 6d). The negative gradient of Y_{ws} near $\theta = 180°$ also contributes to the region of counter-clockwise circulation near the trailing edge of the droplet (solid line, Fig. 6b). When surface tension effects are neglected, due to the counter-rotating flow along the droplet surface (dashed line, Fig. 6b), the water mass fraction is higher at the front of the droplet (dashed line, Fig. 6d).

The numerical simulations presented below begin with a droplet ignition transient similar to the one just described. There are variations in the evaporation time, and the overall time for energy addition and formation of an envelope flame varies between simulations. Reasonable variations in the rate of energy addition during the simulation of the external ignition process

produced negligible differences in the numerical results when plotted as a function of time after ignition.

3.2 Validation

In order to validate the global single step mechanism for methanol combustion used in the present model, a few quasi-steady simulations have been carried out to simulate porous sphere experiments reported in the literature. The extinction velocities predicted by a quasi-steady version of our model have been compared with those obtained experimentally by Sami and Ogasawara [22]. Table 1 shows the values for extinction velocity at different droplet (porous sphere) diameters. The numerical and experimental results are in good agreement.

Furthermore, the transient numerical simulations for $Re_0 = 0.01$ and $d_0 = 0.43$ mm have been compared with the experimental data of Yang et al. [1]. The two cases previously discussed were for methanol droplet combustion in dry air with surface tension effects included and neglected. Since the extent of air humidity has not been reported in [1], a third case, which includes surface tension effects and with 100% relative humidity (RH), has also been simulated.

Figure 7 shows the square of the dimensionless diameter as a function of t_c, the time after an envelope flame has been formed for the three simulations along with the experimental results for four cases from Yang et al. [1]. Thus, $t_c = 0$ s corresponds to the formation of an envelope flame, which is approximately when the experimental data collection begins. Figure 7 shows that all three simulations track the experimental data well for most of the droplet lifetime and seem to approximately follow the d^2-law. The diameter corresponding to the time, when the slope of the $(d/d_0)^2$ curve drastically changes is termed the extinction diameter (d_e). The moment of extinction is derived from the simulations by monitoring flame disappearance. The results for d_e are shown in Table 2.

The extinction diameters for the three simulations vary greatly. The simulation neglecting surface tension effects predicts the smallest extinction diameter at 0.054 mm, followed by the simulation including surface tension effects in dry air at 0.110 mm. The largest extinction diameter of 0.125 mm corresponds to the case of surface tension and saturated ambient air. Comparing these predictions to the experimental results, it is clear that surface tension effects greatly increase the extinction diameter leading to closer agreement with the experimental data. Even though the temporal variation of $(d/d_0)^2$ appears to be similar for all three cases for most of the droplet lifetime, the differences in the extinction diameters and in the evaporation constants are due to differences in water absorption. The effect of surface tension in water absorption will be discussed in detail in later sections.

The difference in the extinction diameter between the experiment ($d_e \approx 0.17$ mm) and the numerical simulations that include surface tension ($d_e = 0.110$ and 0.125 mm) may be due to the use of a single step reaction in the model. The assumption of negligible radiant heat transfer in the present model may also contribute to the difference. However, the initial diameter of the droplet is only 0.43 *mm* and the literature [4] has shown that, for methanol droplets with diameters smaller than 1.5 *mm*, the effect of radiation becomes negligible.

3.3 Effect of Surface Tension

The difference between the extinction diameters for the $Re_0 = 0.01$ and $d_0 = 0.43$ mm in dry air simulations that include and neglect surface tension effects derives from the different major modes of water transport within the droplet. As previously discussed, an envelope flame surrounds the droplet in these two cases at t = 19.2 and 17.4 ms ($t_c = 0$). The envelope flame becomes nearly spherically symmetric at approximately t = 40 ms.

The active combustion period, when surface tension effects are neglected, starts with the formation of an envelope flame at t = 17.4 ms and ends with droplet extinction at approximately t = 320 ms. During the early portion of this period, the counter-clockwise circulation present at t = 17.4 ms (dashed line, Fig. 6b) decreases in magnitude as the flame approaches spherical symmetry. When the flame is nearly spherically symmetric, the major impetus for droplet circulation is the weak convective flow in the gas phase. Thus, flow within the droplet is largely characterized by a weak clockwise circulation superimposed on a strong radial flow caused by rapid vaporization during the majority of the active combustion period. Figure 8, for t = 93.1 ms, shows a typical liquid-phase streamline pattern present during active combustion when surface tension effects are neglected. Figure 9 shows v_θ*, T_s and Y_{ws} for four different times during the active combustion period. The gradients of these quantities are small due to the presence of the nearly spherically symmetric flame. Water that condenses along the droplet surface may either re-vaporize or be transported to the droplet interior. At t = 46.9 ms, Y_{ws} is low (Fig. 9c), with methanol being the primary liquid species at the droplet surface. The droplet surface temperature for this time (Fig. 9b) is therefore below the boiling temperature for methanol (337.8 K) which is much lower than the boiling temperature of water (373.15 K). Thus, the re-vaporization of liquid water at the droplet surface is not significant at this time. Transport of water to the droplet interior is accomplished via molecular diffusion and internal circulation, which are both slow processes when surface tension effects are absent. The result is an increase in Y_{ws} during the combustion period (Fig. 9c). The increase in Y_{ws} eventually allows for values of T_s above the boiling point for methanol (Fig. 9b). At these higher temperatures, vaporization of water at the droplet surface becomes more of a factor, leading to a reduction in T_s (Fig. 9b) and Y_{ws} near extinction (see $\overline{Y}_{ws}$ in Fig. 12).

The case that includes surface tension effects has an active combustion period that starts with the formation of an envelope flame at t = 19.2 ms and ends with extinction at approximately t = 290 ms. Surface tension effects create complex flow patterns within the droplet as the droplet lifetime progresses. Figure 10 shows the liquid-phase streamlines for four different times during the active combustion period. Figure 11 presents the distributions of v_θ*, T_s and Y_{ws} for the same four times. The flow within the droplet consists of several strongly counter-rotating cells which are rapidly changing in number, size, and direction of rotation (Fig. 10). The direction of rotation of each of the cells is indicated by arrows in Fig. 10 and the sign of v_θ* in Fig. 11a. These rotation patterns and directions are also consistent with the water mass fraction profile along the droplet surface shown in Fig. 11c. The gradients in droplet surface temperature (Fig. 11b) are small during the period of active combustion.

As previously discussed, the solutal Marangoni effect becomes increasingly important as the flame surrounds the droplet. A detailed examination of our numerical results indicates that the solutal Marangoni effect is more significant than the thermal Marangoni effect during the active combustion period. For the small surface temperature gradients present under nearly spherically symmetric conditions, the interfacial shear stress equation, which is used to determine v_θ* at the droplet surface, depends primarily upon the gradient of σ along the droplet surface, which can be thought of as the gradient of Y_{ws} along the droplet surface. Therefore, for a tangential surface flow dominated by surface tension effects, there should be a direct relationship between the gradient of Y_{ws} along the droplet surface and v_θ*. This relationship is seen in Figs. 11a and 11c. Each time that the tangential surface velocity is zero, there is a corresponding maximum or minimum in Y_{ws}. It is this variation in Y_{ws}, and therefore σ, which drives the tangential surface flow.

Figure 12a shows the average mass fraction of water in the droplet and the average mass fraction of water along the droplet surface ($\overline{Y}_{ws}$) throughout the droplet lifetime. This figure clearly shows the enhanced transport of water to the droplet interior due to surface tension effects, which results in almost perfect mixing. In contrast, the case neglecting surface tension effects, which undergoes diffusion limited mixing, shows a large difference between the average mass fraction of water in the droplet and $\overline{Y}_{ws}$. The transport of water away from the droplet surface causes $\overline{Y}_{ws}$ for the case with surface tension effects to be lower than the case neglecting surface tension effects, for most of the droplet lifetime. The differing major modes of water transport within the droplet leads to a large difference between the mass fractions of water in the droplet for the two cases. At extinction, the droplet is composed of approximately 74% water by mass when surface tension effects are included and 6% when surface tension effects are neglected. The average mass fraction of water within the droplet continues to increase after extinction due to the preferential vaporization of the more volatile methanol species. Also, at this low initial Reynolds number, residual water vapor left over from combustion remains in the vicinity of the droplet and condenses on the droplet surface.

Figure 12b presents the evaporation constant for the cases with and without surface tension. Including surface tension leads to a higher evaporation constant early in the droplet lifetime due to lower water mass fraction at the droplet surface, compared to the case without surface tension (Fig. 12a). As the mass fraction of water along the droplet surface increases, the evaporation constant for the case including surface tension decreases. This trend is due to the higher latent heat of evaporation of the water compared to that of methanol. The predicted trend is in qualitative agreement with the experimental data of Choi et al. [5]. Quantitative comparison was not pursued due to the different environment surrounding the methanol droplet in [5]. For

the case that neglects surface tension effects, the water mass fraction at the droplet surface increases fast and reaches an equilibrium value (Fig. 12a). As a result, the evaporation constant for this case, after its initial steep increase while the droplet is heating up, remains approximately constant until the flame extinguishes. At a later stage in the droplets' lifetimes, the water mass fraction at the droplet surface for the case with surface tension effects increases very steeply to values much higher than the case that neglects surface tension effects (Fig. 12a). As a result, the droplet that includes surface tension effects extinguishes at a larger diameter.

3.4 Effect of Reynolds Number

Figure 13 presents the time history of the average mass fraction of water in the droplet for d_0 = 0.43 mm and two different initial Reynolds numbers (Re_0 = 0.01 and 5) when surface tension effects are included and neglected. For a given Re_0, including surface tension effects results in enhanced liquid phase mixing and a large increase in the average mass fraction of water in the droplet. As the initial Reynolds number increases, the strength of the droplet circulation caused by the external flow increases, which enhances the liquid phase mixing. However, for the Re_0 = 0.01 case with surface tension effects, there is already near perfect mixing (Fig. 12a). Thus, raising Re_0 from 0.01 to 5 when surface tension effects are included should not appreciably affect water absorption in the droplet. Figure 13 shows this to be true in that (prior to extinction) the rate at which water is absorbed into the droplet is nearly identical for the two cases that include surface tension effects. In contrast, the results for Re_0 = 0.01 and 5 that do not include surface tension effects show a large increase in the amount of water absorbed prior to extinction as Re_0 is increased. For the Re_0 = 5 case without surface tension effects, the transport of water within the droplet is controlled by internal circulation, which is enhanced only due to the higher droplet/gas relative velocity. Consequently, the rates of water absorption with

and without surface tension effects are more similar for $Re_0 = 5$ than $Re_0 = 0.01$. However, even at $Re_0 = 5$, there is a large difference between the amount of water absorbed when surface tension effects are included and neglected. This further indicates that water transport within the droplet is primarily affected by surface tension effects for the range of Re_0 from 0.01 to 5.

Increasing Re_0 from 0.01 to 5 resulted in an increase in the extinction diameter when surface tension effects were both included and neglected. For the cases that included surface tension effects, the extinction diameter went from $d_e = 0.110$ mm when $Re_0 = 0.01$ to $d_e = 0.168$ mm when $Re_0 = 5$. Neglecting surface tension effects produced extinction diameters of $d_e = 0.054$ mm at $Re_0 = 0.01$ and $d_e = 0.166$ mm at $Re_0 = 5$. An increase in Re_0 results in an increase in the rate that oxygen is supplied to the flame front. The higher oxygen supply rate must be balanced by a higher rate of fuel supplied by the droplet surface or oxygen will "leak" through the flame front and cause extinction. As water content builds within the droplet, the maximum rate of fuel that can be made available (via transport from the droplet interior) for vaporization at the droplet surface will decrease and eventually fall below the rate required to balance the oxygen supply. Thus, extinction diameter increases with Re_0.

Figure 13 also shows that the mass fraction of water in the droplet increases only gradually after extinction for the $Re_0 = 5$ cases as compared to the $Re_0 = 0.01$ cases. When $Re_0 = 5$, the strength of convection is such that the residual water vapor surrounding the droplet is rapidly swept downstream. Thus, the gradual increase in water mass fraction after extinction for $Re_0 = 5$ is due to preferential methanol vaporization.

Figures 14a-c present the predicted time histories of a) average droplet surface temperature, b) evaporation constant, and c) dimensionless diameter squared $[(d/d_0)^2]$ for $d_0 = 0.43$ mm and four different initial Reynolds numbers ($Re_0 = 0.01$, 0.1, 1, and 5) when surface

tension effects are included. The results for Re_0 = 0.01 and 0.1 are indistinguishable from each other on the graphs. The numerical predictions in Figs. 14a-c show that varying Re_0 over the range 0.01 to 5 causes only a very small change in the time histories of the displayed quantities during the active combustion period. Only near extinction is there a divergence between the results. As previously discussed, the primary effect of increasing Re_0 is a corresponding increase in d_e (see Fig. 14c). The similarity of the model predictions indicates that combustion of methanol droplets at low initial Reynolds numbers is dominated by surface tension effects.

3.5 Effect of Initial Droplet Diameter

The effect of varying initial droplet diameter on the numerical results for a fixed initial Reynolds number of 0.01 is also discussed. Initial droplet diameters ranging from 0.16 mm to 1.72 mm are considered and surface tension effects are included. Figures 15a-d show a) the average droplet surface temperature, b) the evaporation constant, c) the dimensionless diameter squared $[(d/d_0)^2]$, and d) the average mass fraction of water in the droplet as a function of time scaled with the initial diameter squared for four different initial droplet diameters (d_0 = 0.16, 0.215, 0.43, and 0.86 mm). As the droplet size increases, the total time for the active combustion period increases resulting in greater water absorption (Fig. 15d) and larger extinction diameters [11]. The increasing water concentration and combustion time that accompanies an increase in d_0, allows for heating of the droplet surface to temperatures above the boiling point of methanol (337.8 K) as shown in Fig. 15a. The numerical model predicts that the evaporation constant (K) increases with d_0 (Fig. 15b). The ignition time for each case is indicated by the sharp increase in K toward its maximum value displayed in Fig. 15b and the visible change in slope of $(d/d_0)^2$ that occurs early in the droplet lifetime as seen in Fig. 15c. Figure 15b also shows that the method

used to numerically ignite the droplet gives an ignition time that is of the same order as the period of active combustion for the $d_0 = 0.16$ mm case.

Figure 16 presents a comparison of the predicted dependence of extinction diameter on initial droplet diameter for $Re_0 = 0.01$ both including and neglecting surface tension effects, to the experimental data of Yang et al. [1], Cho et al. [2], and Lee and Law [3]. All three experiments used methanol as the fuel. As cautioned by Dietrich et al. [6], only the drop-tower results of Yang et al [1] were obtained in air while the experiments reported by Cho et al. [2] and Lee and Law [3] were conducted in atmospheres that produced higher burning rates. The experimental data shown in Fig. 16 indicates that the extinction diameter increases approximately linearly with d_0. Our numerical simulations that include surface tension also show an approximately linear dependence. This linear dependence (for methanol droplet combustion in a quiescent environment) is also displayed in the experimental results of Dietrich et al. [6] for methanol droplets ranging from $d_0 = 2$ mm to $d_0 = 5$ mm and predicted in the asymptotic analysis of Zhang et al. [10] in the limit of perfect mixing within the liquid droplet. It has been demonstrated that the complete liquid-phase mixing assumption, as opposed to diffusion-limited mixing, produces numerical results in one-dimensional numerical modeling [11] and asymptotic analysis [10] that are in better agreement with experiment. Our axisymmetric numerical model that includes surface tension effects predicts a time-varying cellular flow within the droplet (Fig. 10) that is consistent with the complete mixing assumption.

Figure 16 also shows that neglecting surface tension effects produces a much different dependence of d_e on d_0. For $d_0 = 0.43$, 0.86, and 1.72 mm, much lower values for d_e are predicted when surface tension effects are neglected. The numerical model predicts that d_e will actually increase with decreasing d_0 for initial diameters less than 0.43 mm. For $Re_0 = 0.01$,

neglecting surface tension effects results in diffusion-controlled mixing which corresponds to a high liquid mass Peclet number (as defined in Marchese and Dryer [11]). The spherically symmetric numerical results of Marchese and Dryer [11] show that, in the limit of large liquid mass Peclet number, d_e may increase with decreasing d_0 in agreement with our results for $d_0 <$ 0.43 mm.

4 Conclusions

The effect of surface tension on the combustion of methanol droplets at low initial Reynolds numbers was studied using a predictive transient, axisymmetric numerical model. Both the initial droplet diameter and the initial Reynolds number were varied to determine their effect on the numerical predictions for combustion in air. The numerical results indicate that, for initial Reynolds numbers as high as 5, surface tension effects play an important role in determining the amount of water absorbed by the droplet and the droplet extinction diameter.

Detailed results for the combustion of a 0.43 *mm* methanol droplet in a nearly quiescent environment were presented. A low initial Reynolds number of 0.01, causing a deviation from spherical symmetry, was used to simulate a nearly quiescent environment. When surface tension effects were neglected, the predicted extinction diameter was much smaller than that obtained experimentally. In the absence of surface tension effects, the liquid-phase mixing is primarily diffusion driven with a very weak liquid-phase circulation for the entire droplet lifetime. When surface tension effects were included, the weak liquid-phase circulation was greatly enhanced and the predicted extinction diameter was much closer to experimental results. Including surface tension effects resulted in a complex, time-varying, multi-cellular flow structure within the droplet. These complex liquid-phase flow patterns, which result in nearly perfect mixing, occur

very early in the droplet lifetime and exist until the end of the lifetime. The surface tension gradients that drive the complex flow during active droplet combustion are primarily due to the solutal Marangoni effect. The enhanced mixing results in greater water absorption which leads to a higher extinction diameter.

For combustion in a nearly quiescent environment, including surface tension effects resulted in an approximately linear variation of the extinction diameter with the initial droplet diameter, which is in agreement with theoretical predictions and experimental measurements.

Acknowledgements

This research was funded by NASA EPSCoR under grant NCC5-572. Computational resources were provided by the Thermal-Fluids computational facility and the Research Computing Facility at the University of Nebraska – Lincoln.

5 References

[1] J.C. Yang, G.S. Jackson, and C.T. Avedisian, Proc. Combust. Inst., 23 (1990) 1619-1625.

[2] S.Y. Cho, M.Y. Choi, and F.L. Dryer, Proc. Combust. Inst., 23 (1990) 1611-1617.

[3] A. Lee and C.K. Law, Combust. Sci. Tech., 86 (1992) 235-265.

[4] A.J. Marchese, F.L. Dryer, R.O. Colantonio, and V. Nayagam, Proc. Combust. Inst., 26 (1996) 1209-1217.

[5] M.Y. Choi, S.Y. Cho, F.L. Dryer, and J.B. Haggard, Eastern States Section Meeting, The Combustion Institute, Albany NY, Paper No.73 (1989) 1-4.

[6] D.L. Dietrich, J.B. Haggard, *Jr.*, F.L. Dryer, V. Nayagam, B.D. Shaw, and F.A. Williams, Proc. Combust. Inst., 26 (1996) 1201-1207.

[7] K. Okai, O. Moriue, M. Araki, M. Tsue, M. Kono, J. Sato, D.L. Dietrich, and F.A. Williams, Combust. Flame, 121 (2000) 501-512.

[8] H. Hara, and S. Kumagai, Proc. Combust. Inst., 25 (1994) 423-430.

[9] B.D Shaw, Combust. Flame, 81 (1990) 277-288.

[10] B.L Zhang, J.M. Card, and F.A. Williams, Combust. Flame, 105 (1996) 267-290.

[11] A.J. Marchese, and F.L. Dryer, Combust. Flame, 105 (1996) 104-122.

[12] I. Aharon, and B.D. Shaw, Phys. Fluids, 8 (1996) 1820-1827.

[13] H.A. Dwyer, I. Aharon, B.D. Shaw, and H. Niazmand, Proc. Combust. Inst., 26 (1996) 1613-1619.

[14] H.A. Dwyer, B.D. Shaw, and H. Niazmand, Proc. Combust. Inst., 27 (1998) 1951-1957.

[15] H.A. Dwyer, and B.D. Shaw, Combust. Sci. Tech., 162 (2001) 331-346.

[16] A.T. Shih, and C.M. Megaridis, Int. Journal of Heat and Mass Transfer, 39 (2) (1996) 247-257.

[17] D.N. Pope and G. Gogos, Numerical Heat transfer, Part B, 48 (2005) 213-233.

[18] D.N. Pope and G. Gogos, Combust. Flame, 142 (2005) 89-106.

[19] D.N. Pope, D. Howard, K. Lu and G. Gogos, AIAA J. of Thermo. Heat Trans., 19 (3) (2005) 273-281.

[20] D. Howard, D.N. Pope and G. Gogos, Proceedings of the Fourth Joint Meeting of the U.S. Sections of the Combustion Institute, Philadelphia, PA, (2005).

[21] V. Raghavan, V. Babu, T. Sundararajan, and R. Natarajan, Int. Journal of Heat and Mass Transfer, 48 (2005) 5354-5370.

[22] H. Sami, and M. Ogasawara, JSME. Bulletin, 13 (1970) 395-404.

[23] R.C. Reid, J.M. Prausnitz, and B.E. Poling, The Properties of Gases and Liquids, McGraw-Hill Inc., New York, 1987.

[24] K. Kurihara, M. Nakamichi, and K. Kojima, Am. Chem. Soc., 38 (1993) 446-449.

[25] B.J. McBride, G. Sanford, and M.A. Reno, Coefficients for calculating thermodynamic and transport properties of individual species, NASA Tech. Memorandum 4513, 1993.

[26] A.S. Teja, Am. Chem. Soc., 28 (1983) 83-85.

[27] A.S. Teja, and P. Rice, Ind. Eng. Chem. Fundam., 20 (1981) 77-81.

[28] N.B. Vargaftik, Y.K. Vinogradov, and V.S. Yargin, Handbook of Physical Properties of Liquids and Gases: Pure Substances and Mixture, Begell House, Inc., New York, 1996.

[29] B.M.S. Santos, A.G.M. Ferriera and I.M.A. Fonseca, Fluid Phase Equilibrium, 208 (2003) 1-21.

[30] C.H. Westbrook, and F.L. Dryer, Combust. Sci. Tech., 27 (1981) 31-43.

[31] S.V. Patankar, Numerical Heat Transfer and Fluid Flow, Hemisphere Publishing Corp., New York, 1980.

[32] J.P. Van Doormal, and G.D. Raithby, Num. Heat Trans., 7 (1984) 147-163.

[33] M. Vinokur, J. Comp. Phys., 50 (1983) 215-234.

LIST OF TABLES

LIST OF FIGURES

d (mm)	Extinction Velocity (m/s)	
	Numerical Results	Sami & Ogasawara [22] experiments
5	1.01	1.18
10.1	1.57	1.49

Table 1. Comparison of extinction velocity obtained from numerical and experimental results

Case	Relative Humidity (%)	d_e (mm)
Numerical, no surface tension	0	0.054
Numerical, surface tension	0	0.110
Numerical, surface tension	100	0.125
Experiment	Not reported	0.16-0.19

Table 2. Comparison of predicted and measured extinction diameters

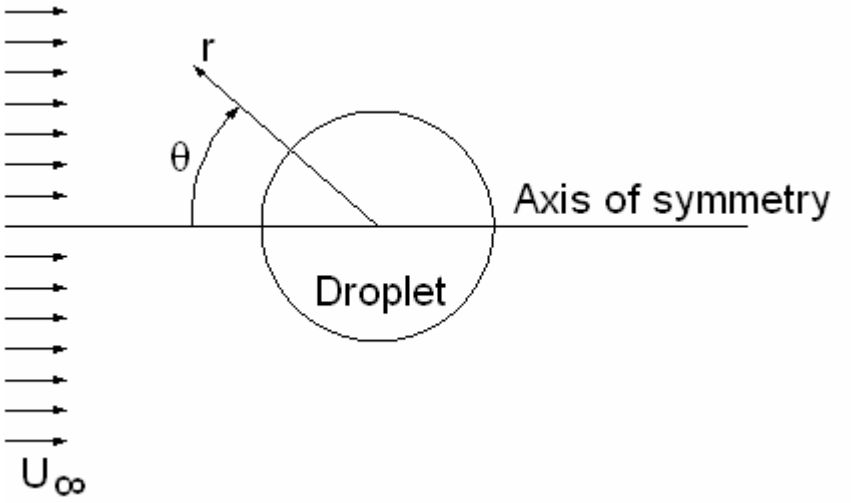

Figure 1: Problem schematic

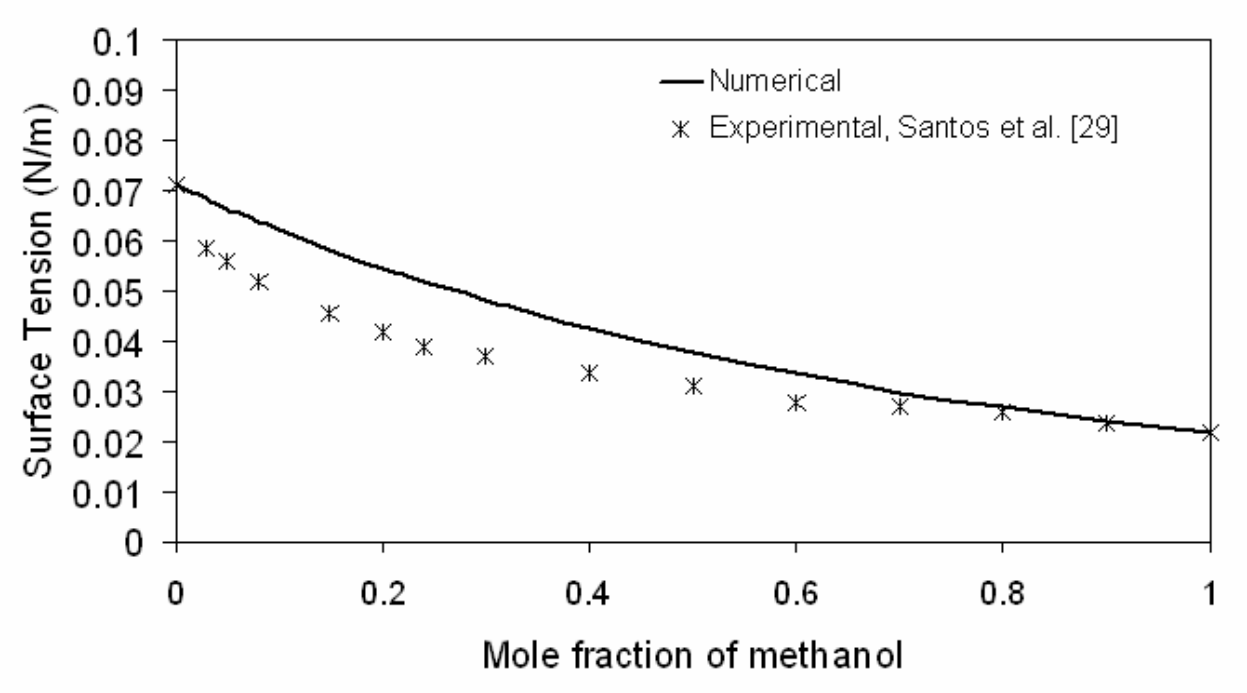

Figure 2: Surface tension variation with composition for a water/methanol mixture in air at 303.15 K.

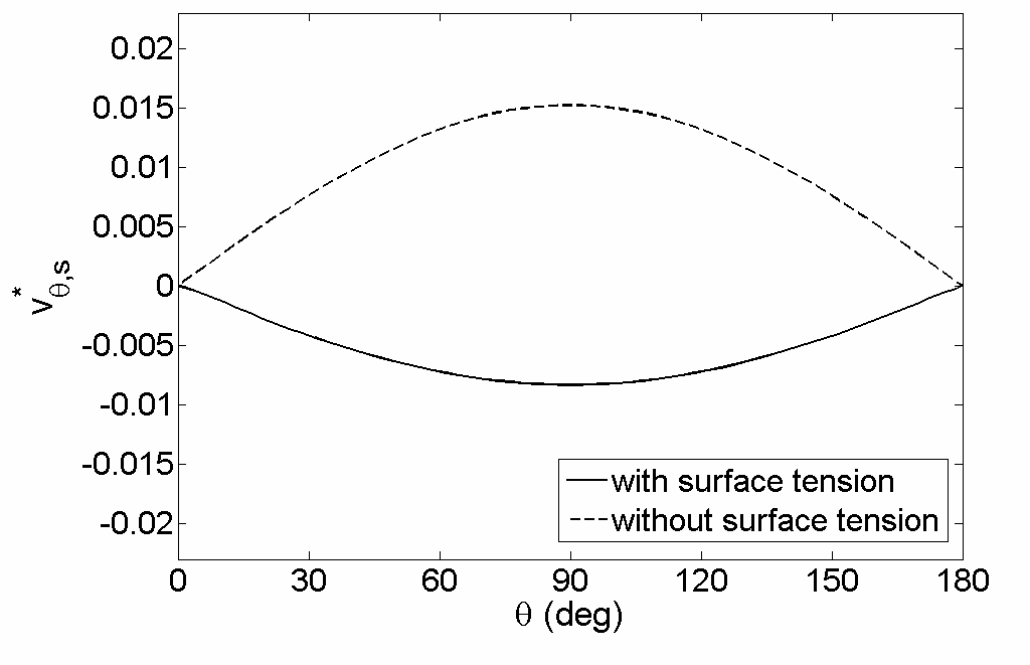

(a)

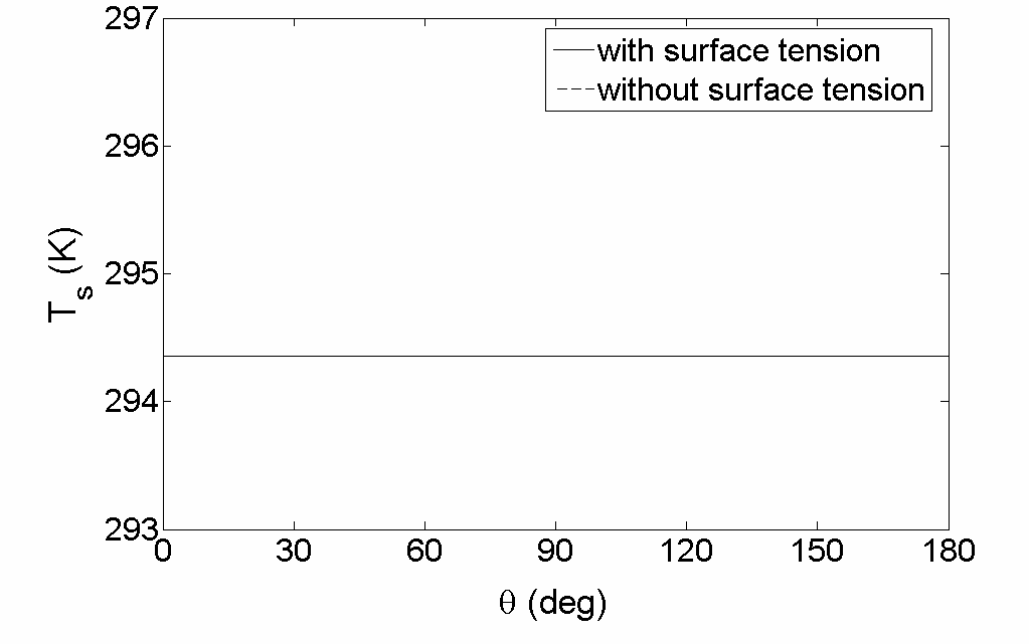

(b)

Figure 3: Droplet surface distributions at t ≈ 1.3 ms for (a) dimensionless tangential velocity, and (b) temperature; d_0 = 0.43 mm, Re_0 = 0.01.

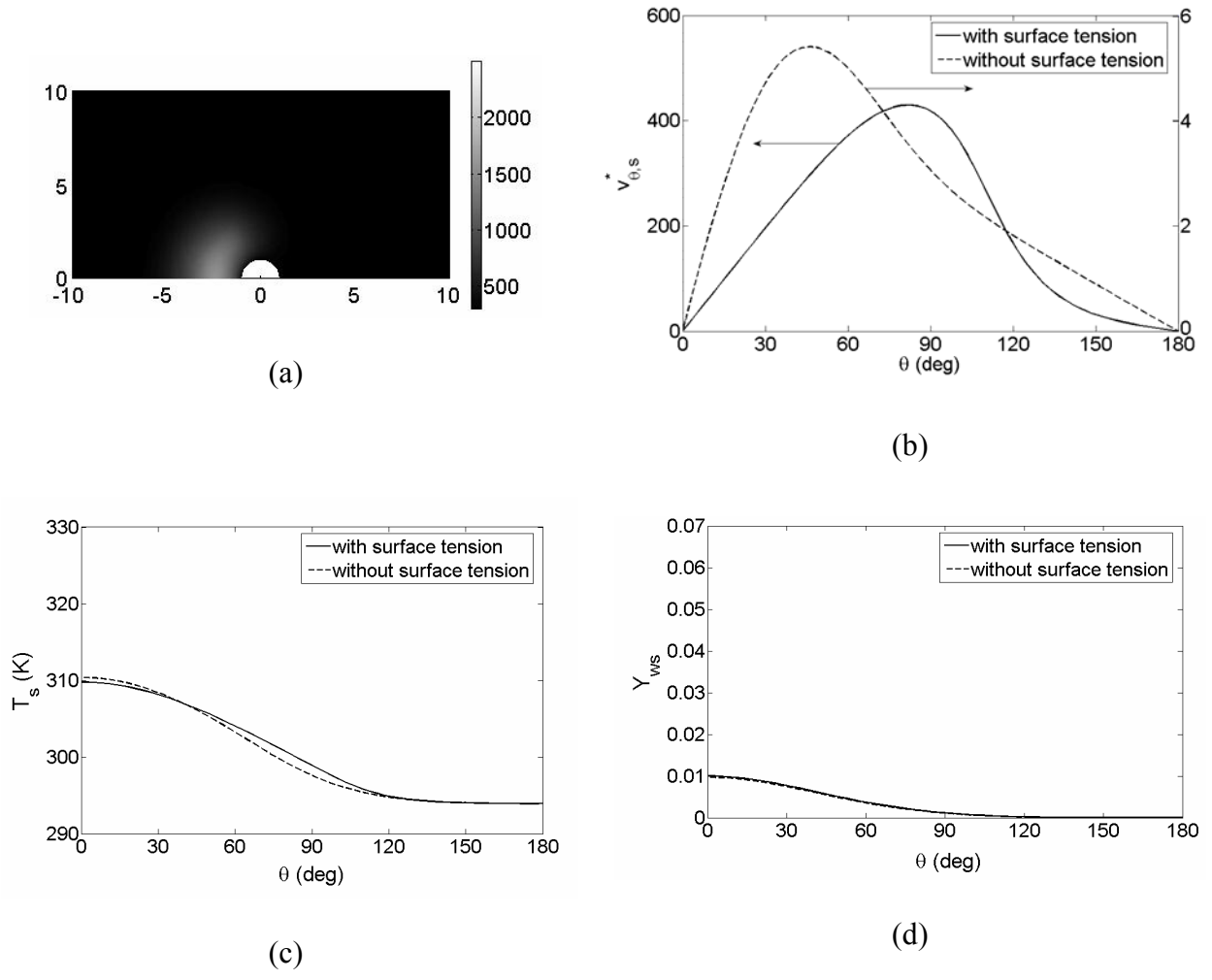

Figure 4: Numerical predictions at t ≈ 3 ms for d_0 = 0.43 mm and Re_0 = 0.01; (a) grayscale plot of temperature distribution in K for case without surface tension effects, and distribution along droplet surface of (b) dimensionless tangential velocity, (c) temperature, and (d) water mass fraction

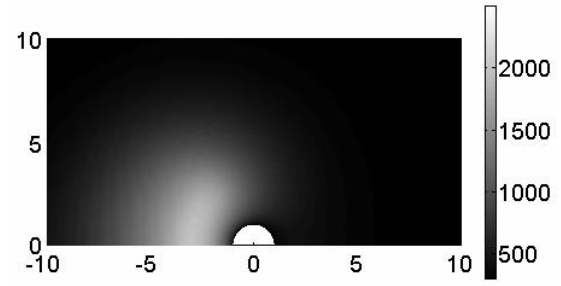

(a)

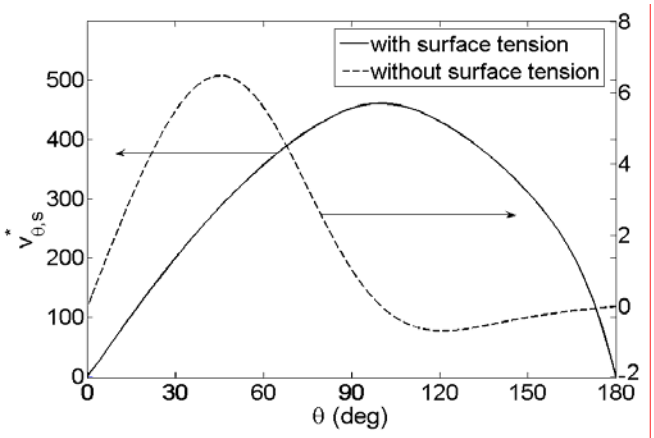

(b)

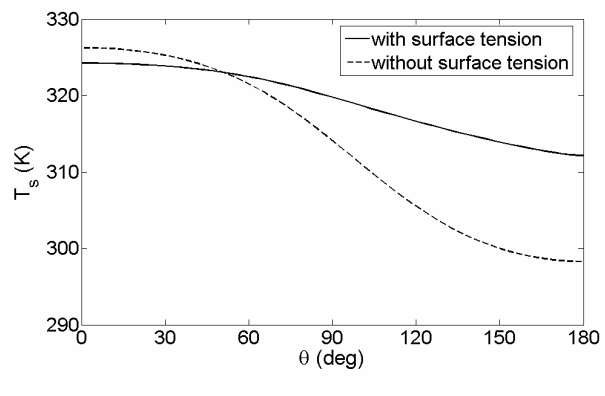

(c)

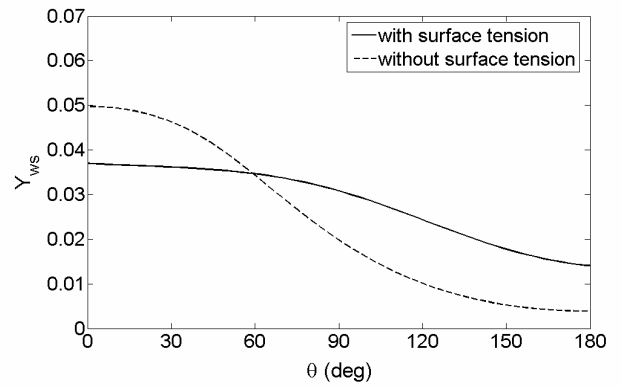

(d)

Figure 5: Numerical predictions at the end of energy addition for d_0 = 0.43 mm and Re_0 = 0.01; (a) grayscale plot of temperature distribution in K for case without surface tension effects, and distribution along droplet surface of (b) dimensionless tangential velocity, (c) temperature, and (d) water mass fraction; t = 16.4 ms with surface tension effects, t = 12.7 ms without.

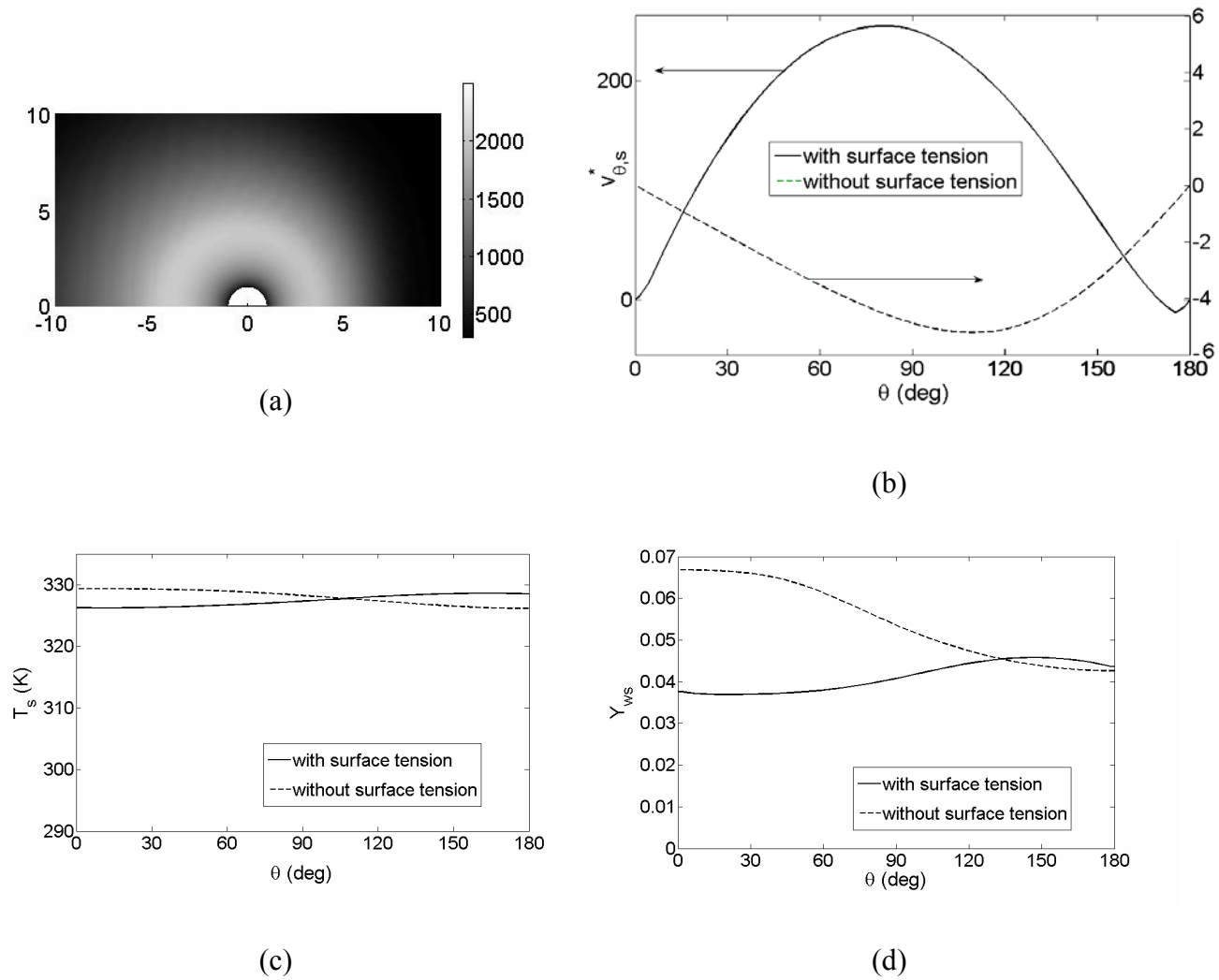

Figure 6: Numerical predictions at the formation of an envelope flame for d_0 = 0.43 mm and Re_0 = 0.01; (a) grayscale plot of temperature distribution in K for case without surface tension effects, and distribution along droplet surface of (b) dimensionless tangential velocity, (c) temperature, and (d) water mass fraction; t = 19.2 ms with surface tension effects, t = 17.4 ms without.

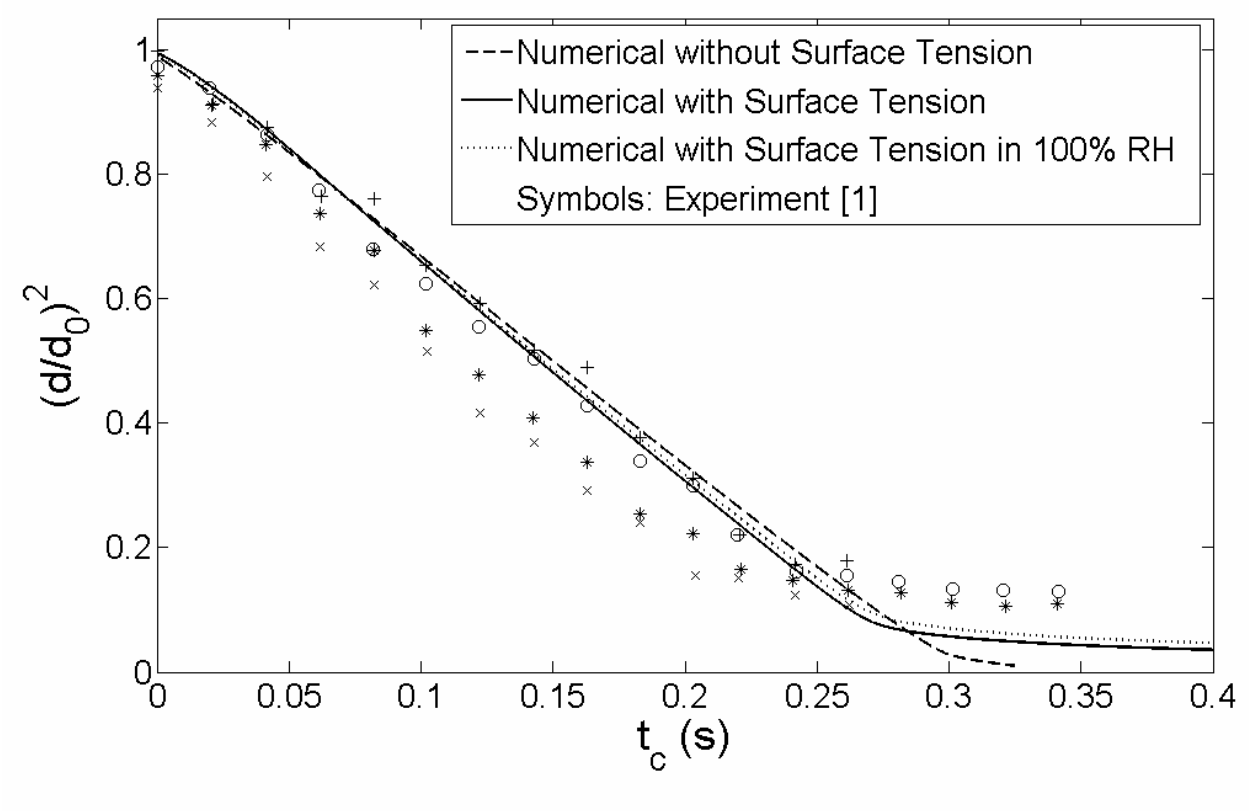

Figure 7: Dimensionless diameter squared versus time (t_c); numerical and experimental results.

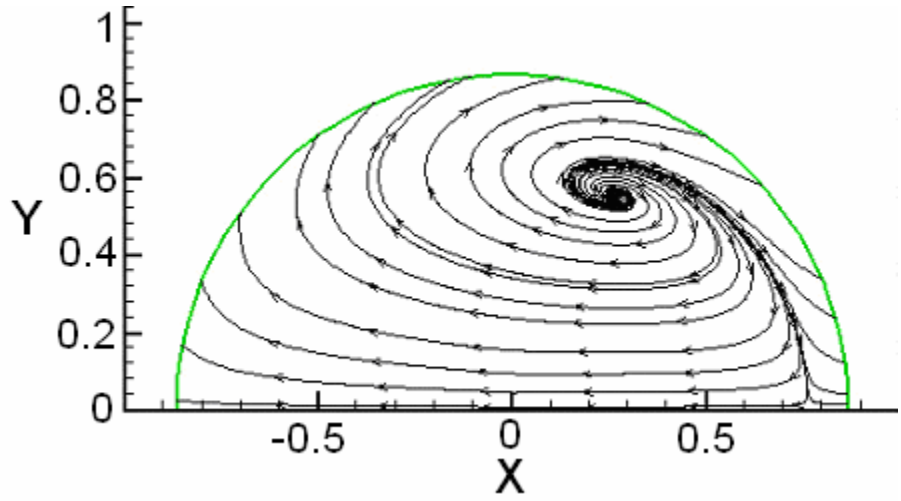

Figure 8: Typical liquid-phase streamlines during active combustion phase without surface tension effects; t = 93.1 ms.

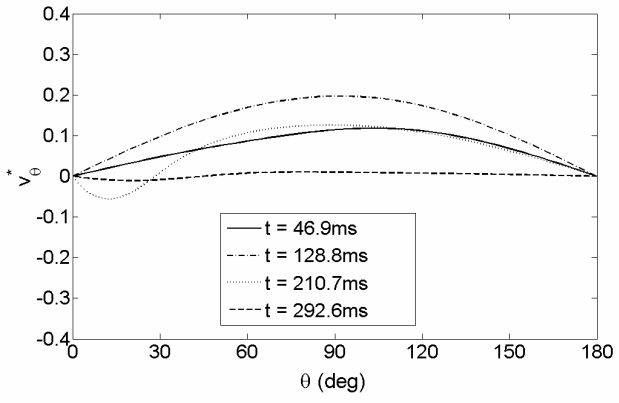

(a)

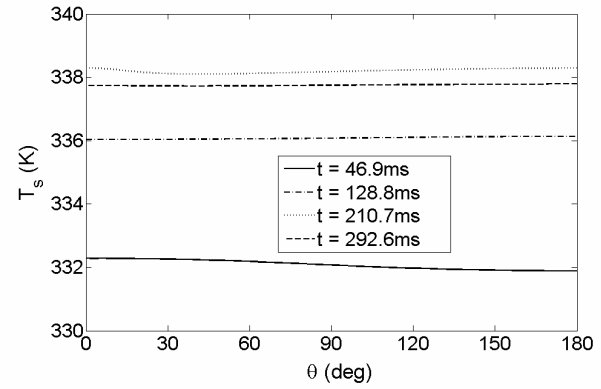

(b)

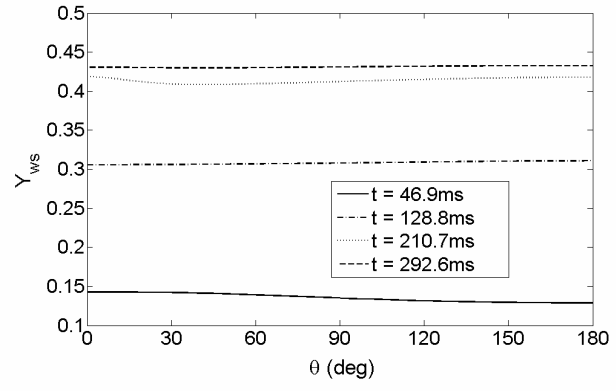

(c)

Figure 9: Droplet surface distributions at various times during the active combustion phase for (a) dimensionless tangential velocity, (b) temperature and (c) water mass fraction; d_0 = 0.43 mm, Re_0 = 0.01, without surface tension effects.

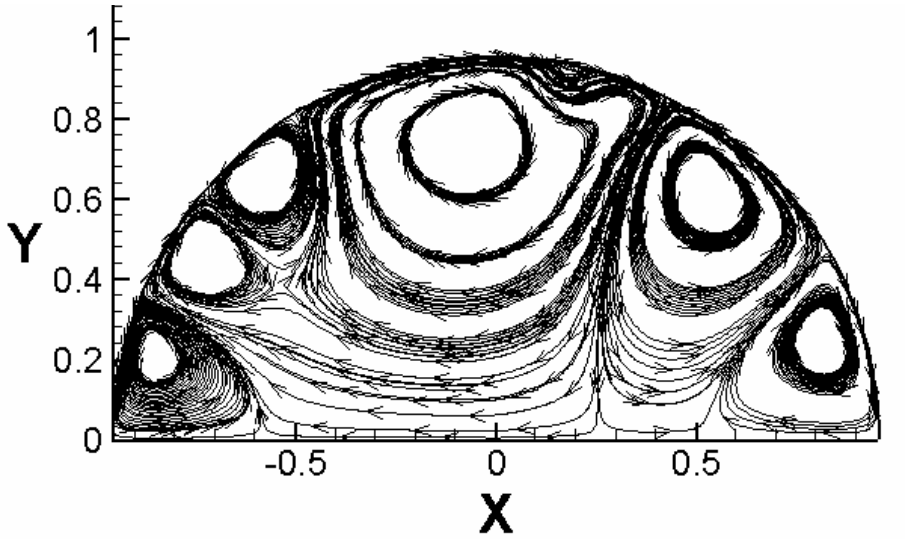

(a)

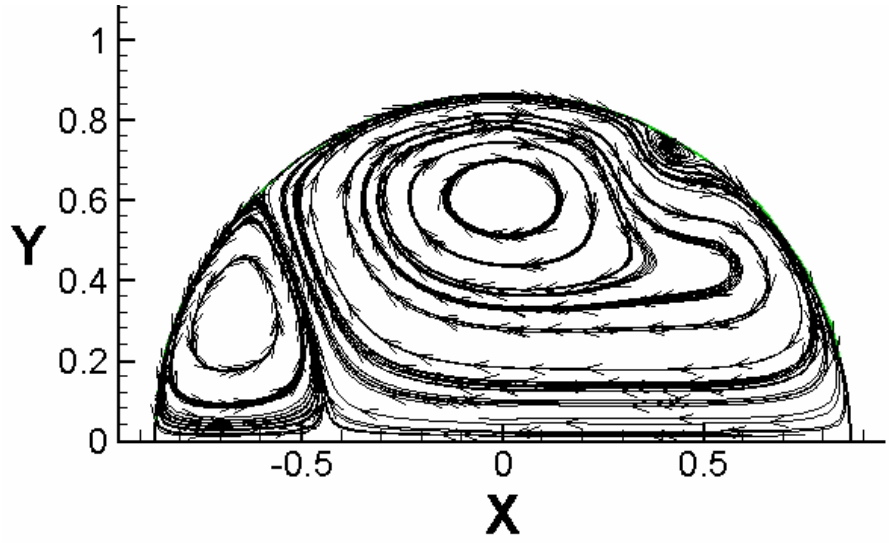

(b)

Figure 10 a&b: Liquid-phase streamlines at various times during the active combustion phase; d_0 = 0.43 mm, Re_0 = 0.01, with surface tension effects, (a) t=46.9 ms and (b) t= 93.1 ms

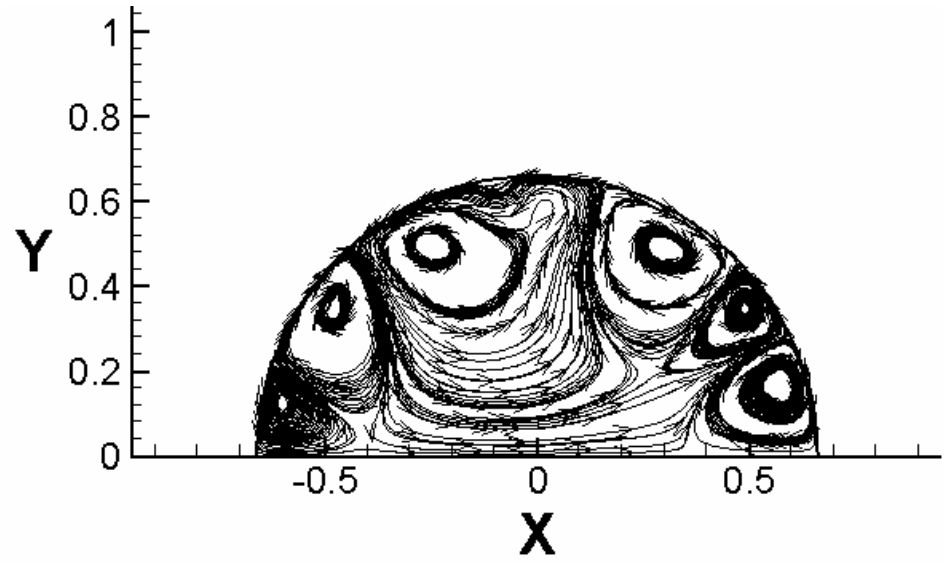

(c)

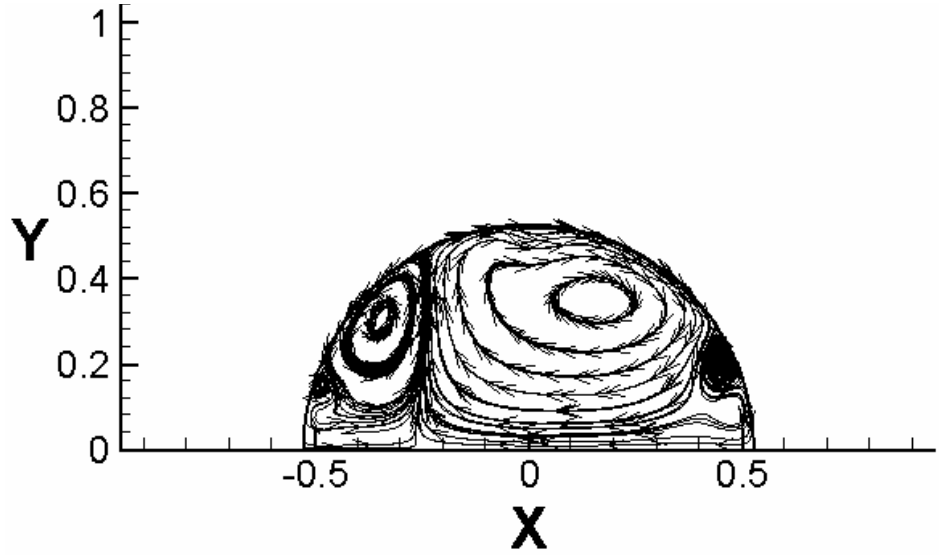

(d)

Figure 10 c&d: Liquid-phase streamlines at various times during the active combustion phase; d_0 = 0.43 mm, Re_0 = 0.01, with surface tension effects, (c) t=180.0 ms and (d) t=226.2 ms.

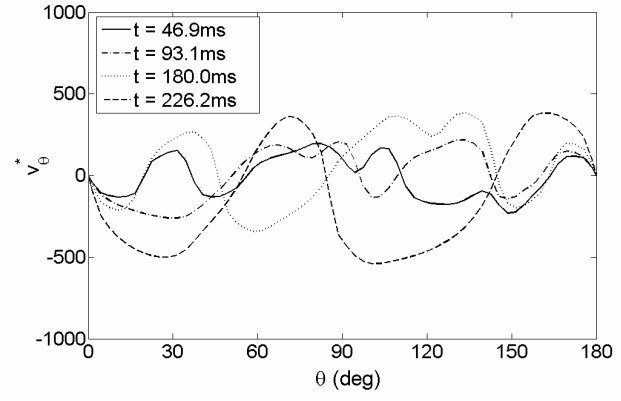

(a)

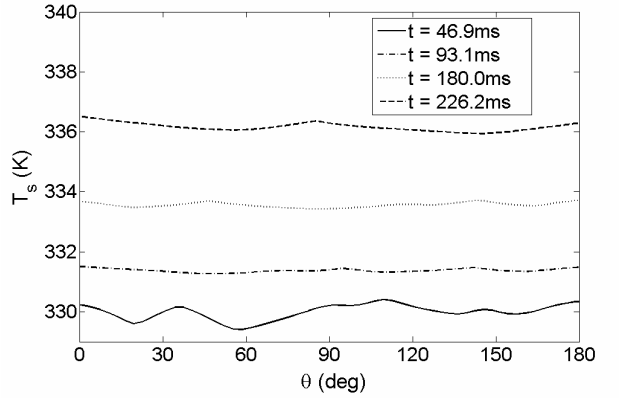

(b)

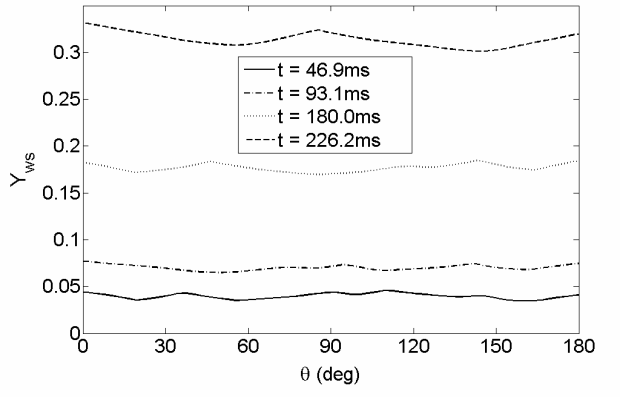

(c)

Figure 11: Droplet surface distributions at various times during the active combustion phase for (a) dimensionless tangential velocity, (b) temperature and (c) water mass fraction; d_0 = 0.43 mm, Re_0 = 0.01, with surface tension effects.

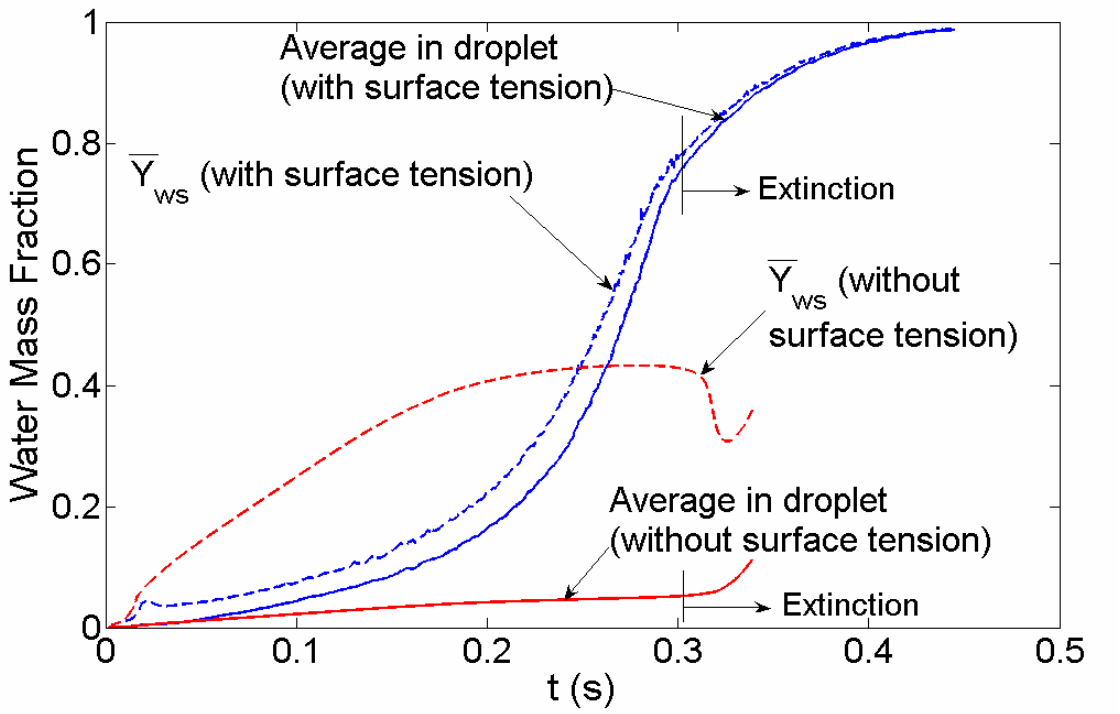

Figure 12a: Average water mass fraction in liquid droplet and average surface mass fraction; d_0 = 0.43 mm, Re_0 = 0.01.

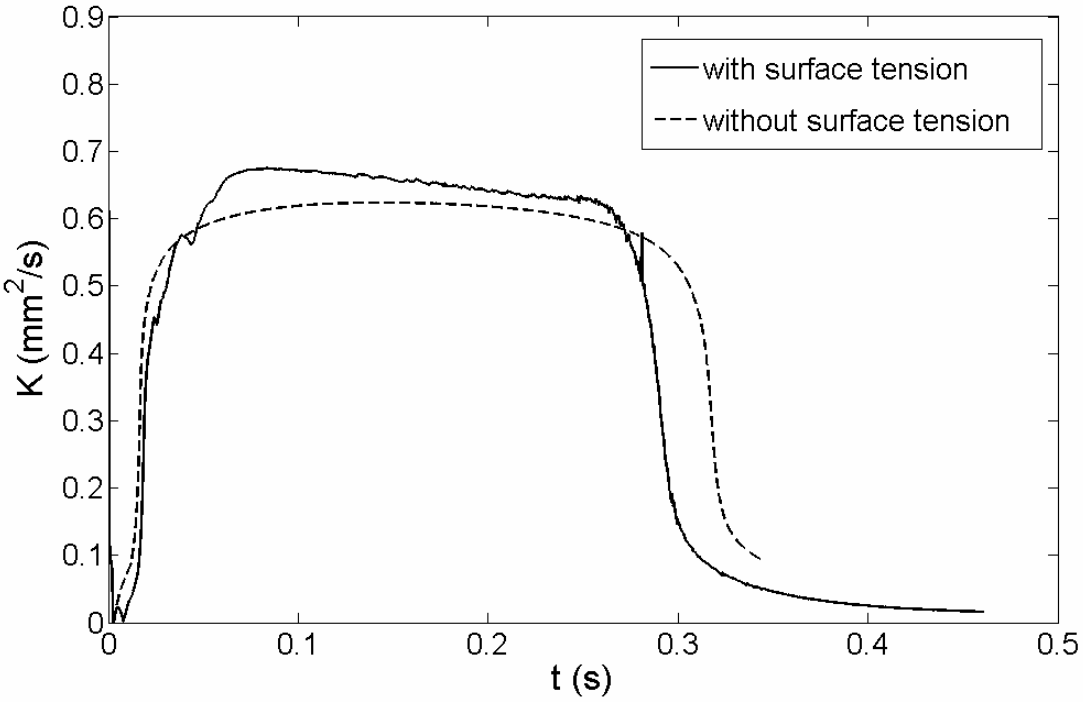

Figure 12b: Evaporation constant versus time; numerical results; d_0 = 0.43 mm, Re_0 = 0.01

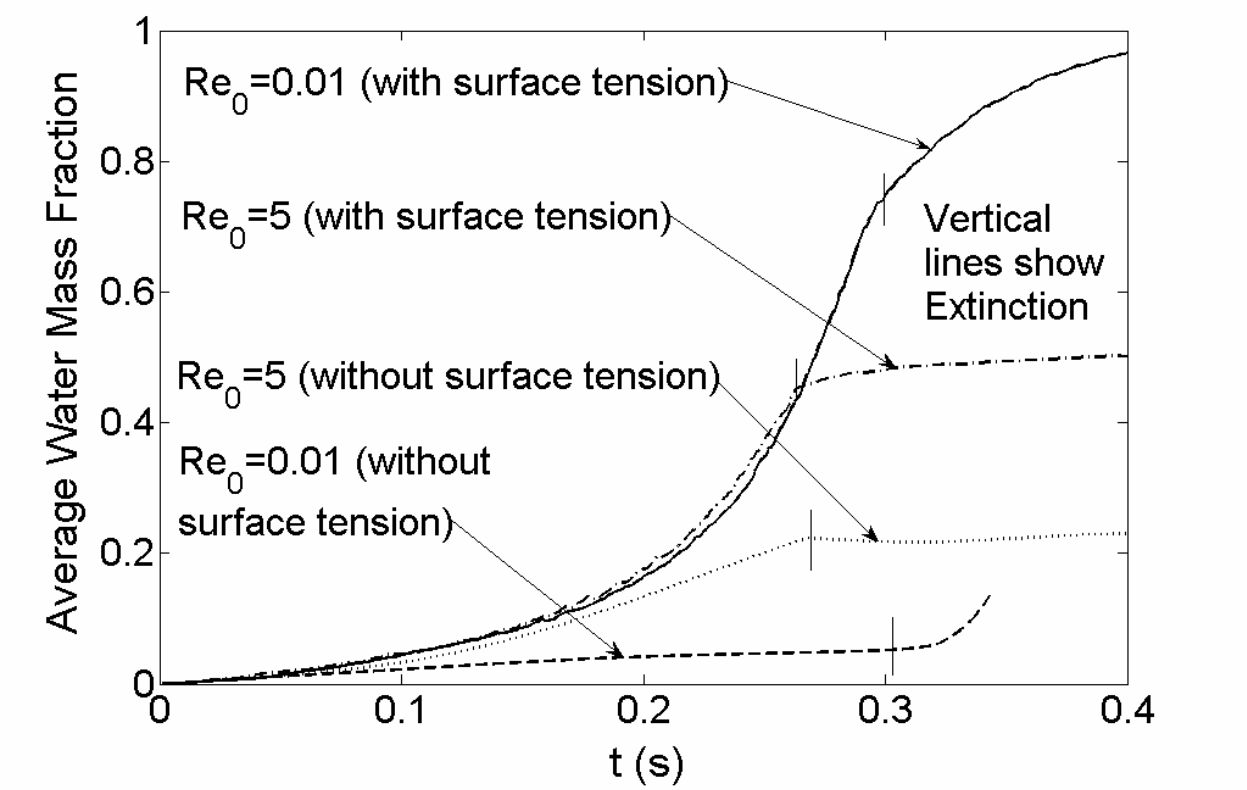

Figure 13: Average water mass fraction in droplet for Re_0 = 0.01 and Re_0 = 5; d_0 = 0.43 mm.

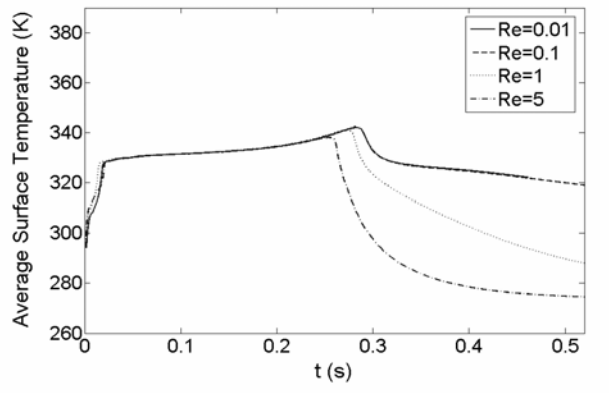

(a)

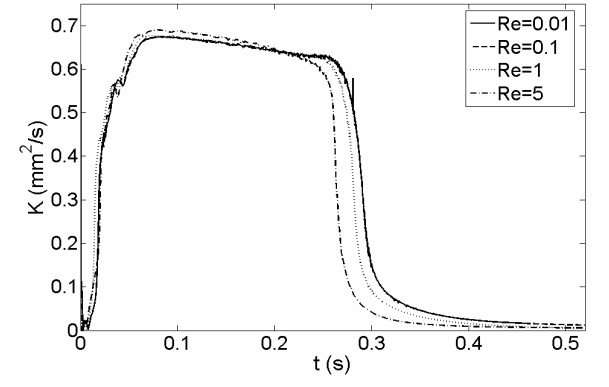

(b)

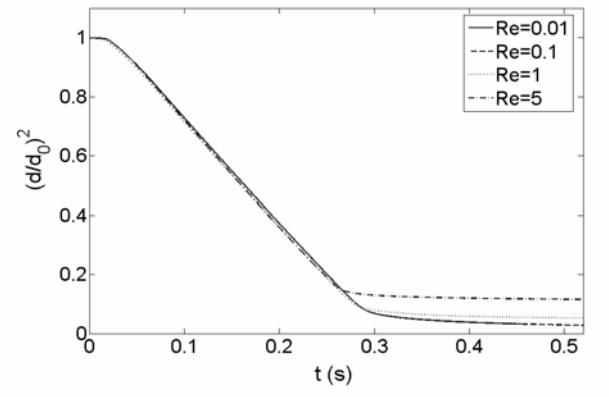

(c)

Figure 14: Time histories of a) average droplet surface temperature, b) evaporation constant, and c) dimensionless diameter squared $[(d/d_0)^2]$; d_0 = 0.43 mm, Re_0 = 0.01, 0.1, 1, and 5, with surface tension effects.

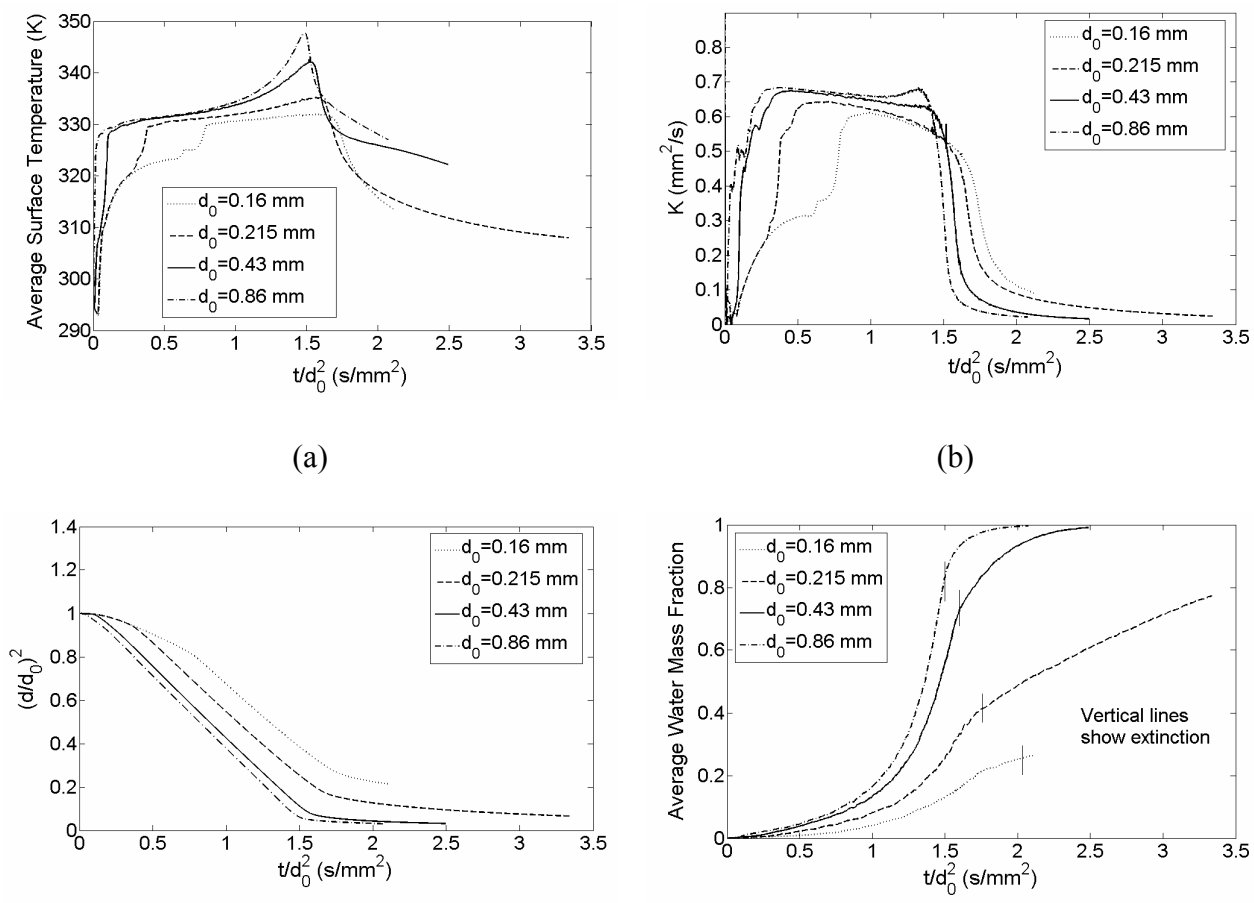

Figure 15: a) average droplet surface temperature, b) evaporation constant, c) dimensionless diameter squared [$(d/d_0)^2$], and d) average mass fraction of water in the droplet as a function of (t/d_0^2); d_0 = 0.16, 0.215, 0.43, and 0.86 mm, Re_0 = 0.01, with surface tension effects.

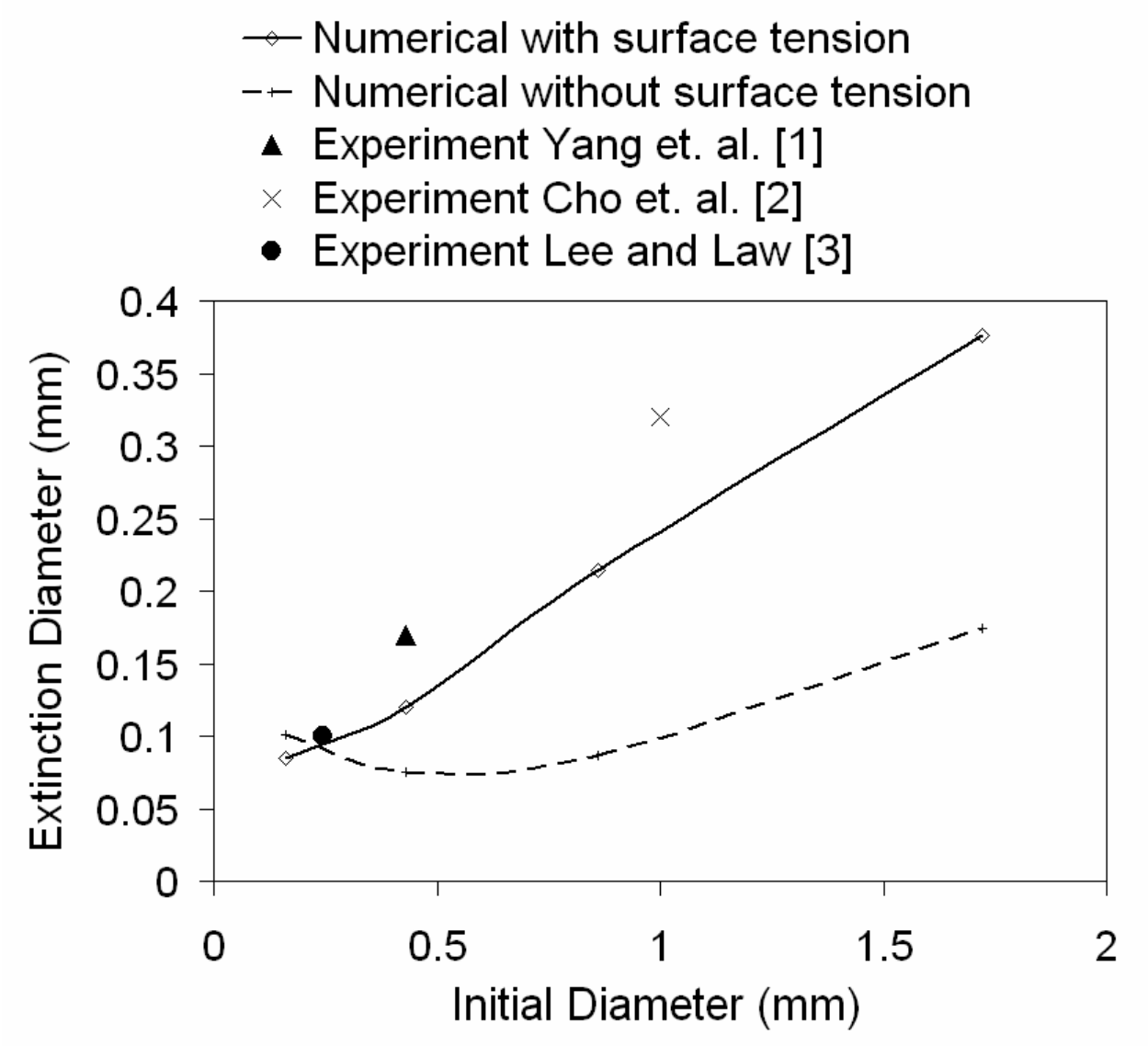

Figure 16: Extinction diameter versus initial droplet diameter; $Re_0 = 0.01$.